









Environmental effects on layer-dependent dynamics of Dirac fermions in quasicrystalline bilayer graphene

Y. Zhao,¹ T. Suzuki ¹, T. Iimori,¹ H.-W. Kim ², J. R. Ahn,^{2,3} M. Horio,¹ Y. Sato,¹ Y. Fukaya ⁴, T. Kanai ¹, K. Okazaki,¹ S. Shin ¹, S. Tanaka ⁵, F. Komori ^{1,*}, H. Fukidome,⁶ and I. Matsuda ¹

¹*Institute for Solid State Physics (ISSP), The University of Tokyo, Kashiwa, Chiba 277-8581, Japan*

²*Department of Physics and SAINT, Sungkyunkwan University, Suwon, Gyeonggi-do 16419, Republic of Korea*

³*Samsung-SKKU Graphene Centre, Sungkyunkwan University, Suwon, Gyeonggi-do 440-746, Republic of Korea*

⁴*Advanced Science Research Center, Japan Atomic Energy Agency, Tokai, Ibaraki 319-1195, Japan*

⁵*Department of Applied Quantum Physics and Nuclear Engineering, Kyushu University, Fukuoka-shi, Fukuoka, 819-0395, Japan*

⁶*Research Institute of Electronic Communication, Tohoku University, Sendai, Miyagi 980-8577, Japan*



(Received 18 September 2021; revised 22 February 2022; accepted 28 February 2022; published 16 March 2022)

The carrier dynamics in various types of epitaxial graphene layers on SiC substrates was investigated by means of time- and angle-resolved photoemission spectroscopy (ARPES). Layer-dependent electron doping was observed in the Dirac bands of quasicrystalline bilayer graphene after optical pumping, leading to generation of transient voltage between the upper and lower layers. The amount of photoinduced carrier transport depends on the distance from the substrate. A comparison of the ARPES results of single-layer graphene between flat and stepped SiC substrates experimentally indicates that a source of the doping carriers likely originates from interface step states. The dynamic model is described based on the electronic structure, calculated using density functional theory.

DOI: [10.1103/PhysRevB.105.115304](https://doi.org/10.1103/PhysRevB.105.115304)

I. INTRODUCTION

The dynamical behavior of carriers in graphene has attracted academic interest to investigate the temporal evolution of massless Dirac fermions and also to fulfill technical needs in the development of the next-generation optoelectronic devices [1–7]. A comprehensive understanding has been pursued by direct observations of the electronic states by time- and angle-resolved photoemission spectroscopy (ARPES) [8–14]. Using optical pulses, photoexcited carriers in graphene layers were traced in real time, and the dynamics was described by various elementary processes, such as electron-phonon coupling and supercollision [8–14]. Recently, twisted bilayer graphene was synthesized and showed intriguing properties [15–19], i.e., superconductivity at a twisted angle of 1.1° and quasicrystallinity at 30° . This novel material has opened the new research field of “twistronics” [20]. ARPES measurements on epitaxial quasicrystalline bilayer graphene (QCBG) discovered transient voltage between the two layers that was not expected theoretically [21]. The experimental reasoning has indicated possible contributions from the substrate, but the detailed scenario has remained unknown.

Figure 1(a) shows schematic drawings of epitaxial graphene on a Si-face SiC substrate. The crystal surface is covered with a buffer layer, and a graphene layer is located on it with a distance of $d_1 = 3.3 \text{ \AA}$ [22,23]. As shown in Fig. 1(b), QCBG is also prepared on a buffer layer with $d_2 = 3.35 \text{ \AA}$

for the lower graphene layer and with $d_3 = 6.81 \text{ \AA}$ for the upper one [18], as determined by positron diffraction experiments [24,25]. In both cases, the layers are electronically n type with the Fermi level (μ_{eq}) located at the energy μ above the Dirac point (DP). Compared with a freestanding layer of nondoped graphene, the epitaxial graphene layer is complicated with various external factors, i.e., interface, substrate, and doping. Thus it is required to investigate the environmental effect to reveal the dynamics of Dirac fermions in reality.

In the present research, we performed ARPES measurements on various systems of single-layer and bilayer graphene on Si-face SiC substrates to extensively study the carrier dynamics. In QCBG, we observed the temporal evolution of photoexcited carriers in Dirac cones that were asymmetric between the upper and lower layers and quantitatively described by the transient doping from the interface. Experimental comparisons of ARPES results between the graphene layers on a flat SiC substrate and the graphene layers on a stepped one indicate that the doped carriers in epitaxial graphene likely originate from Si and/or C step states at the interface. This assignment is theoretically supported by the interface electronic structures, calculated by density functional theory (DFT).

II. EXPERIMENT

Single-layer graphene and bilayer graphene are epitaxially grown on a SiC crystal surface by heat treatments [26–32]. Preparations of QCBG were described elsewhere [17]. In brief, a hexagonal boron nitride (h-BN) layer is initially grown on SiC substrate at 1050°C in borazine gas, and it is replaced with a graphene layer by subsequent heating at 1600°C . Further annealing drives growth of the lower graphene layer that

*Present address: Institute of Industrial Science, The University of Tokyo, Tokyo 153-8505, Japan.

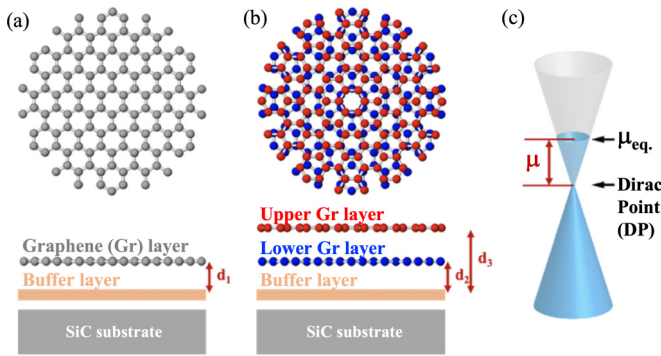


FIG. 1. Top and side views of structure models of (a) single-layer graphene and (b) QCBG on a SiC(0001) substrate. Small gray, red, and blue circles denote C atoms in different layers, while d_1 , d_2 , and d_3 denote the interlayer distance between the buffer layer and graphene layers. (c) Electronic structure of the Dirac cone in n -type graphene. The Dirac point and equilibrium chemical potential are denoted as DP and μ_{eq} , respectively. The red “ μ ” denotes the energy level between the Dirac point and the equilibrium chemical potential.

has a 30° -rotated orientation from the upper graphene layer, consequently forming QCBG on a buffer layer, as shown in Fig. 1(b). Single-layer graphene on a stepped SiC surface is synthesized by heat treatments of the vicinal $6H$ -SiC(0001) crystal (4° off toward $[11\bar{2}0]$) in the N_2 atmosphere. The detailed procedure is described elsewhere [33].

All the graphene samples, after being introduced in the ultrahigh-vacuum chamber, were cleaned by annealing at 400°C . The quality and crystallinity were confirmed by patterns of low-energy electron diffraction and valence band spectra of photoemission spectroscopy. Static spectra of angle-resolved photoemission spectroscopy (ARPES) were taken by a helium discharge lamp ($h\nu = 21.2\text{ eV}$). TARPES measurements were made by the pump-probe method [34]. Using a high-harmonic-generation system based on a femtosecond-pulse Ti:sapphire laser, a beam at $h\nu = 1.55\text{ eV}$ was used as a pump, while the one at $h\nu = 21.7\text{ eV}$ was adopted as a probe. The total time resolution was 70 fs during the experiment.

III. RESULTS AND DISCUSSION

A. Quasicrystalline bilayer graphene

The electronic structure of a graphene layer is composed of Dirac cones at the K and K' points in the Brillouin zone. In QCBG, the upper and lower layers are rotated 30° from each other, and they individually keep the Dirac bands at equilibrium, as shown in Fig. 2. The samples are n type, and the chemical potential μ is referred from the DP. By controlling the 1600°C annealing time for 30 or 20 min, we could prepare two types of samples: those with equivalent and inequivalent μ values between the upper layer Dirac cone (ULD) and the lower layer Dirac cone (LLD), respectively. Figures 2(a) and 2(b) show the equivalent case, $\mu = 0.33\text{ eV}$ in both the ULD and LLD, while Figs. 2(c) and 2(d) correspond to the inequivalent one, $\mu = 0.23\text{ eV}$ for the ULD and $\mu = 0.31\text{ eV}$ for the LLD. The energy positions of the Dirac points were determined by crossings of the linear dispersion curves of

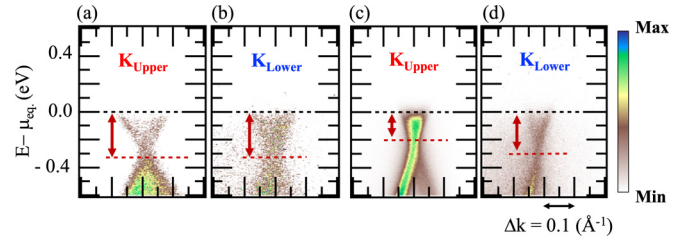


FIG. 2. Photoemission band diagrams of (a) and (c) the upper layer Dirac cones (ULDs) and (b) and (d) the lower layer Dirac cones (LLDs) for two types of QCBG samples: those with (a) and (b) equivalent and (c) and (d) inequivalent μ values between ULD and LLD. The data were taken under the equilibrium condition by a He discharge lamp. Red dashed lines denote the DP positions, while red arrows indicate the amount of μ . A unit of momentum, Δk , is given in the figure.

the Dirac bands. The upper layer of the inequivalent QCBG sample has a smaller μ value than the other layers. This is likely due to remanent acceptor-type defects on the layer that can be removed by long annealing time. A comparison of these two samples should provide an effect of layer-dependent values of μ .

Figure 3 presents temporal variations of the band diagrams of the QCBG sample with equivalent μ_{eq} values. One can find the photoinduced population (depopulation) of carriers in the unoccupied (occupied) Dirac bands and the following relaxation [21]. It is of note that the results of the ULD appear clearer than those of the LLD due to the photoemission probing depth. To extract the time dependence of the physical quantities, the band diagrams are integrated over the momentum range to obtain energy distribution curves (EDCs) at each delay time [10,21]. The collection is given in Fig. 4, showing the apparent time dependence. Each EDC is curve fitted with the Fermi-Dirac distribution function to extract the electron temperature T and chemical-potential shift $\Delta\mu$ [10,21]. In brief, the

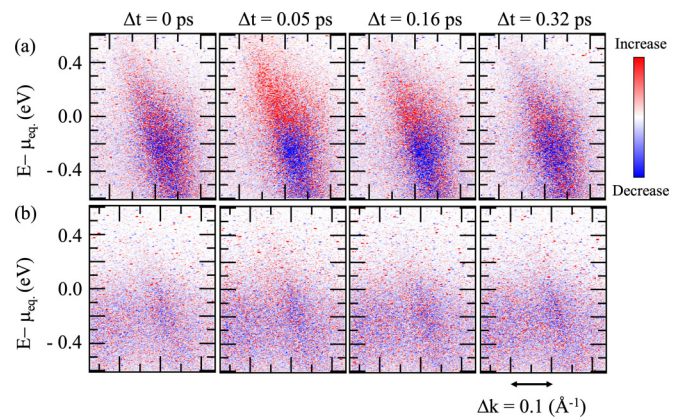


FIG. 3. A series of nonequilibrium band diagrams of the QCBG sample with equivalent μ_{eq} values, taken at various delay times Δt , for the (a) ULD and (b) LLD. The data are expressed as the difference between the TARPES spectra before and after optical pumping. Red and blue points represent increased and decreased photoemission intensity, respectively.

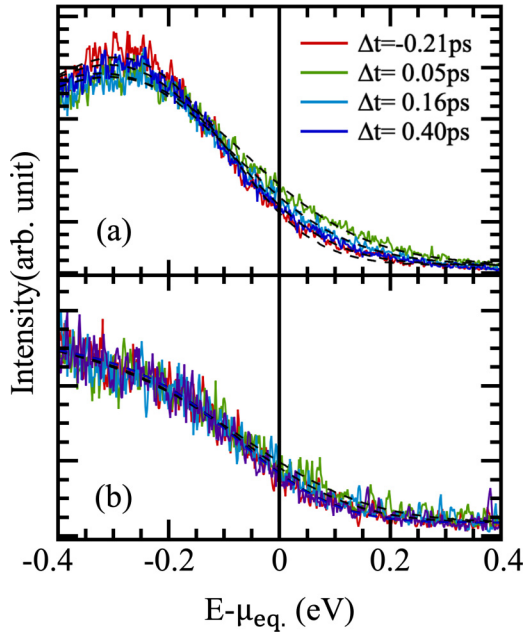


FIG. 4. Energy distribution curve (EDC) in the (a) ULD and (b) LLD in QCBG. Dashed curves are fitting curves using the Fermi-Dirac distribution function.

fitting process was conducted by a polynomial function, $C_1 * \{C_2 + C_3(E - \mu) + f(E - \mu, T) \otimes g(E)\}$, where $f(E - \mu, T) = \frac{1 + C_4(E - \mu)}{1 + \exp(-\frac{E - \mu}{k_B T})}$ is the Fermi-Dirac distribution function and $g(E) = \frac{1}{\sqrt{(2\pi)\sigma}} \exp(-\frac{E^2}{2\sigma^2})$ is the Gaussian function that contains the instrumental resolution σ . After determining the parameters, C_i 's and σ , from spectra of the samples before the optical pumping, TARPES spectra were robustly curve fitted by two parameters, T and μ . The temporal changes in the parameters are plotted in Figs. 5(a) and 5(b). The electron temperature increases by the optical pumping and decays with delay time. The $\Delta\mu$ values appear opposite between the ULD and LLD: positive in the LLD and negative in the ULD. These results are consistent with a previous paper that reported data of a QCBG sample with inequivalent μ values between the ULD and LLD [21]. The experimental findings indicate that the photoinduced ultrafast carrier dynamics in QCBG does not depend on the initial status of μ .

Using experimental values of the electron temperature and the chemical shift, one can derive the temporal variation of the carrier density, Δn , by combining the density of states (DOS) of the graphene Dirac bands with the Fermi-Dirac function [21]. Figure 5(c) plots the experimental value of Δn_{el} at each delay time, decaying with time after the pumping. As listed in Table I, the decay time constants were similar between the electronic temperature and Δn_{el} . To unveil the detailed mechanism, we adopted the following rate equation that is associated with the intra- and interlayer dynamics of photoexcited carriers [21]:

$$\begin{aligned} \frac{dn_{el}^{UL}}{dt} &= -\frac{n_{el}^{UL}}{\tau_{UL}} + \gamma_1(n_{el}^{LL} - n_{el}^{UL}) + G_1 e^{-\frac{t^2}{T_p^2}}, \\ \frac{dn_{el}^{LL}}{dt} &= -\frac{n_{el}^{LL}}{\tau_{LL}} - \gamma_1(n_{el}^{LL} - n_{el}^{UL}) \end{aligned}$$

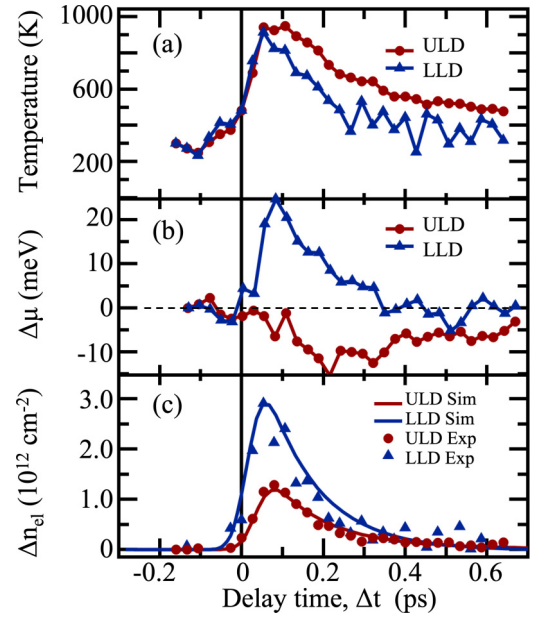


FIG. 5. Time dependence of (a) electronic temperature, (b) chemical-potential shift $\Delta\mu$, and (c) electron density variation Δn_{el} in the ULD and LLD of QCBG. The ULD and LLD are represented in red and blue, respectively. In (c), experimental results are shown as symbols, whereas calculation results found by solving rate equations are shown as curves. Sim, simulated.

$$\begin{aligned} & -\gamma_2(n_{el}^{LL} - n_{el}^{Sub}) + G_2 e^{-\frac{t^2}{T_p^2}}, \\ n_{el}^{LL} + n_{el}^{UL} + n_{el}^{Sub} &= \text{const}, \end{aligned}$$

where n_{el}^{UL} (n_{el}^{LL}) and τ_{UL} (τ_{LL}) are the electron density and decay time in the graphene upper layer (lower layer), respectively. n_{el}^{Sub} is the electron density in the SiC substrate or interface. We imposed conservation of the number of carriers during the dynamical change with time. G_1 (G_2) is a coefficient of the pump-induced net density flux from the SiC substrate or interface to the upper layer (from the substrate or interface to the lower layer). The G_i parameter is phenomenological and contains various elementary processes to realize transient doping in the epitaxial graphene layer. The quantity γ_1 (γ_2) is a rate constant of carrier transfer from the lower layer to the upper layer (from the lower layer to the SiC substrate or interface). T_p is a pulse width (70 fs in the full width at half maximum) of the optical pumping. As shown in Fig. 5(c), the numerical simulation reproduced the experimental result successfully with the values of the parameters listed in Tables I and II. One can find that the two types of samples resulted in $\gamma_1 > \gamma_2$, indicating that the carrier transport between graphite layers (UL and LL) is faster than that between the graphene and the SiC substrate.

In Table I, values of $\Delta\mu$ for a graphene layer are given for comparison. The experimental $\Delta\mu$ is recalled from Ref. [10], and expected values are calculated based on the linear density of states of the Dirac bands [10]. With increasing electron temperature, $\Delta\mu$ becomes negative [10]. Since the Dirac cones are preserved in the QCBG samples, one expects $\Delta\mu < 0$. Unexpectedly, $\Delta\mu$ values are both negative and positive, depending on the layers in the QCBG. This result indicates

TABLE I. Relationships of parameters in single-layer graphene and quasicrystalline bilayer graphene (QCBG). The decay time constant of temperature, τ , was obtained by an exponential fit. The equivalent- and inequivalent- μ samples are labeled by “(1)” and “(2),” respectively.

| Parameter | Single-layer graphene [10] | Quasicrystalline bilayer graphene | | | |
|--|----------------------------|-----------------------------------|---------------------|--------------------|---------------------|
| | | Upper(1) | Upper(2) | Lower(1) | Lower(2) |
| μ_{eq} , referred from the Dirac point | 0.39 | 0.33 | 0.23 | 0.33 | 0.31 |
| Experimental $\Delta\mu$ (maximum temperature) | −30 meV (1000 K) | −15 meV (948 K) | −10 meV (1200 K) | +25 meV (914 K) | +30 meV (1200 K) |
| Expected $\Delta\mu$ (maximum temperature) | −30 meV (1000 K) | −34 meV (948 K) | −68 meV (1200 K) | −31 meV (914 K) | −56 meV (1200 K) |
| Decay time constant of temperature (τ) | 0.380 ps | 0.425 ps | 0.133 ps | 0.258 ps | 0.141 ps |
| Decay time constant of Δn (τ_{UL} or τ_{LL}) | | 0.203 ps | 0.156 ps | 0.158 ps | 0.140 ps |

that the transient voltage is generated between two graphene layers and it appears in the QCBG samples of the equivalent- μ case and also the inequivalent- μ one [21]. Increase in the chemical potential most likely indicates carrier transfer to the graphene layers from the substrate or interface. Positive G_i ($i = 1, 2$) values are consistent with the existence of such transient charge transfer in both types of the QCBG sample. Moreover, one can find $G_2 > G_1$, indicating that it is larger in the LL than in the UL with the ratio $G_1/G_2 \approx 0.4$ – 0.6 . To deepen our understanding of the interlayer carrier transport, we adopted the carrier transport model that is associated with an exponential decay by distance, as typically used in the tunneling or ballistic regime [35]. The model indicates that the G_i value is proportional to the exponential function, $\exp(-2\kappa d_i)$, where d_i is the distance to the graphene layer and κ is the decay length of an electronic state that donates carriers to graphene. The model provides that $G_1/G_2 = \exp\{-2\kappa(d_3 - d_2)\}$, and insertion of the d_i value in Fig. 1 results in a κ value of ~ 0.074 – 0.13 \AA^{-1} . The inverse, $\kappa^{-1} \approx 7.6$ – 14 \AA , roughly estimates a size of the wave function that can donate the transient carriers to the graphene overlayers. From the structure models in Fig. 1, the electronic states are reasonably assigned to those located at the height of the buffer and the topmost SiC layers at the interface. Under the Bardeen transfer Hamiltonian model [35], the carrier transport occurs since a tail of the interface wave function extends to the graphene layers.

B. Nontwisted bilayer graphene

To examine the existence of the carrier transfer to the bilayer graphene from the interface, we prepared a sample of the n -type nontwisted bilayer graphene (NTBG), shown in Figs. 6(a) and 6(b), and conducted the TARPES measurement.

TABLE II. Optimized parameters in the rate equations of quasicrystalline bilayer graphene (QCBG) samples with different chemical-potential levels between the UL and the LL. The equivalent- and inequivalent- μ samples are labeled by “(1)” and “(2),” respectively.

| Parameter | QCBG(1) | QCBG(2) |
|------------|--|--|
| γ_1 | $1.6 \pm 0.1 \text{ ps}^{-1}$ | $1.5 \pm 0.1 \text{ ps}^{-1}$ |
| γ_2 | $1.0 \pm 0.1 \text{ ps}^{-1}$ | $0.5 \pm 0.1 \text{ ps}^{-1}$ |
| G_1 | $(2.4 \pm 0.1) \times 10^{13} \text{ cm}^{-2} \text{ ps}^{-1}$ | $(5 \pm 0.1) \times 10^{13} \text{ cm}^{-2} \text{ ps}^{-1}$ |
| G_2 | $(6 \pm 0.1) \times 10^{13} \text{ cm}^{-2} \text{ ps}^{-1}$ | $(8 \pm 0.1) \times 10^{13} \text{ cm}^{-2} \text{ ps}^{-1}$ |

Total-reflection high-energy positron diffraction (TRHEPD) research revealed that the distance to the lower layer is $d'_2 = 3.33 \text{ \AA}$, while the distance to the upper layer is $d'_3 = 6.62 \text{ \AA}$, taking similar values to those of QCBG [18]. Thus NTBG is expected to have carrier doping to the graphene layers from the interface. Figures 6(c) and 6(d) show the time dependence of the electronic temperature and chemical-potential shift $\Delta\mu$. The results are consistent with a previous report [21]. Since the DOS of NTBG is constant with energy, the transient chemical potential essentially remains constant. By taking a close look, one can find the positive $\Delta\mu$ value by the optical pumping, indicating the possible existence of carrier doping in graphene from the interface or substrate.

C. Single-layer graphene on a stepped substrate

Between the layers of graphene and the SiC, there is a buffer carbon layer that terminates the SiC surface, as illustrated in Figs. 1 and 6, but Si dangling bonds (DBs) partially remain at the interface [36]. The area density of Si DBs at the interface corresponds to the order of 10^{15} cm^{-2} , whereas the DOS in single-layer graphene is only on the order of $\sim 10^{12}$ – 10^{13} cm^{-2} near the Dirac point [21]. Thus one might arrive at the conclusion that the electron density from Si DB is large enough to induce the carrier injection from the SiC substrate to the graphene layers and to make the positive chemical shift after the optical pumping. However, the result of the single-layer graphene was negative as reported previously [10] and listed in Table I. Thus it is necessary to seek a different origin at the interface.

To make comparisons, we prepared the epitaxial graphene on a stepped substrate (4° -off vicinal crystal) and performed the TARPES measurement. The graphene layer is n type, and the Dirac point is energetically located at $\mu = 0.4 \text{ eV}$, which

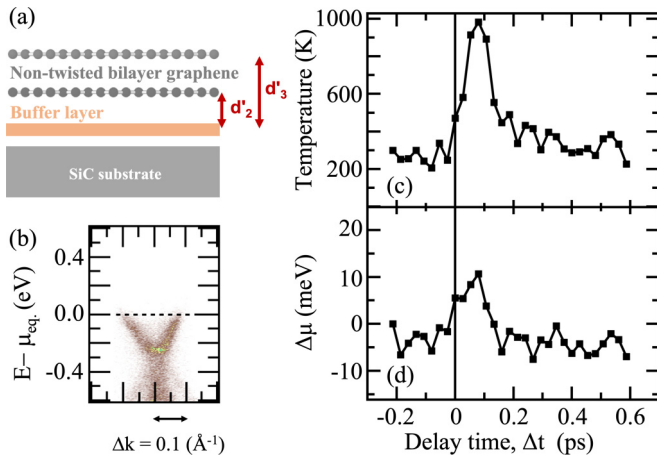


FIG. 6. TARPES results in nontwisted bilayer graphene (NTBG). (a) Side views of structure models of NTBG on a SiC(0001) substrate. (b) Equilibrium angle-resolved photoemission spectra for NTBG at the K point. (c) and (d) Time dependence of electronic temperature and chemical-potential shift $\Delta\mu$.

is close to those of epitaxial graphene and the QCBG on a flat substrate (as shown in Fig. 8). Thus the system is suitable to explore the substrate effect. The single-layer graphene is located on a wide-terrace area of the buffer layer and also on a step region, as illustrated in Fig. 7(a). Orientations along and perpendicular to the step are expressed in the figure and confirmed by low-energy electron diffraction (LEED) observation [Fig. 7(b)].

Figure 8 shows the equilibrium and nonequilibrium photoemission band diagrams at the K and K' points. One can confirm the electronic structure and trace the temporal variations clearly. Following the same procedures of the data analysis [10,21], the electron temperature and the chemical-potential shifts are derived experimentally as plotted in Figs. 9(a) and 9(b), respectively. In contrast to the case of single-layer graphene on a flat SiC surface [10], $\Delta\mu$ is positive on single-layer graphene on the stepped substrate.

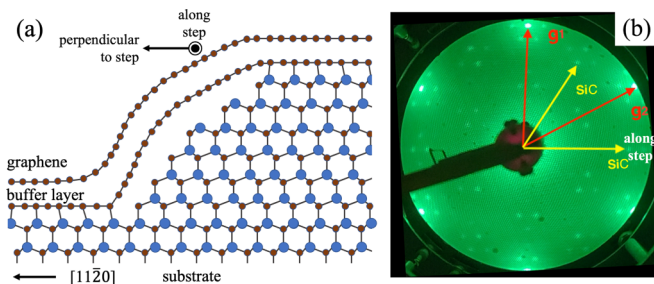


FIG. 7. (a) Cross-section structure model of graphene on a stepped SiC substrate, where blue circles are Si atoms and brown circles are carbon atoms. (b) The LEED pattern of graphene on a stepped substrate. Graphene spots are expressed as g_1 and g_2 , while red arrows show the reciprocal lattice primitive vectors. SiC spots and vectors are shown in yellow.

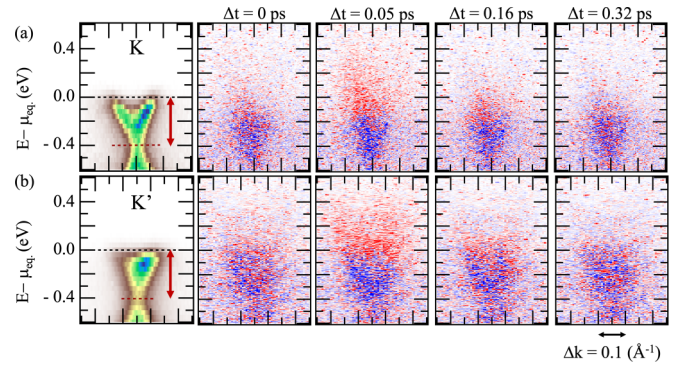


FIG. 8. (a) Equilibrium angle-resolved photoemission spectra in K and K' of graphene on a stepped substrate. (b) The difference spectra in K and K' of graphene on a stepped substrate by TARPES. Red and blue points represent increasing and decreasing photoemission electron intensity, respectively.

To make the further quantitative analysis, we modified the rate equation, as follows, to match with the system.

$$\frac{dn_{el}^G}{dt} = -\frac{n_{el}^G}{\tau_G} - \gamma(n_{el}^G - n_{el}^{Sub}) + Ge^{-\frac{t^2}{\tau_p^2}}, \quad n_{el}^G + n_{el}^{Sub} = \text{const},$$

where n_{el}^G is the electron density with electron lifetime τ_G . The experimental Δn_{el} curve in Fig. 9(c) is reproduced by the parameters listed in Table III.

The temporal parameters confirmed the existence of the transient carrier doping to the graphene layer, and the source is likely the same as in the QCBG case due to the similar

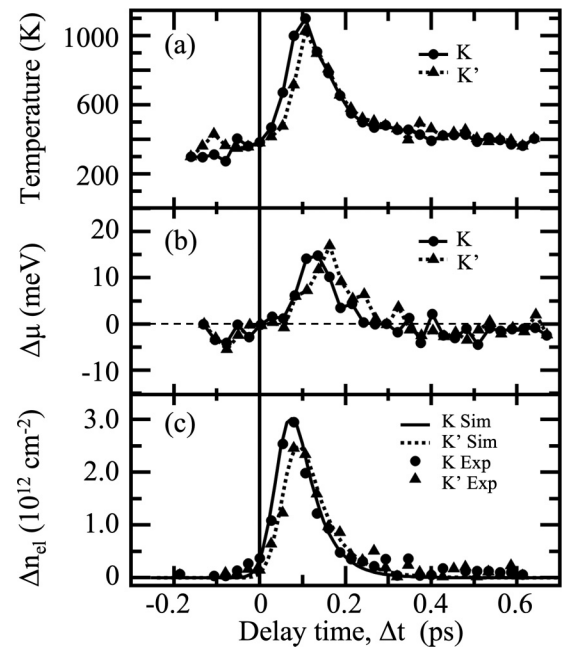


FIG. 9. Time dependence of (a) electronic temperature, (b) chemical-potential shift $\Delta\mu$, and (c) electron density variation Δn_{el} , at the K and K' points of graphene on a stepped substrate. K and K' are represented as solid and dashed curves, respectively. Experimental results are shown as symbols, whereas calculation results found by solving rate equations are shown as curves.

TABLE III. Temporal parameters for single-layer graphene on the stepped SiC substrate.

| Parameter | Single-layer graphene on stepped substrate | |
|--|--|--|
| | K | K' |
| μ_{eq} , referred from the Dirac point | 0.40 eV | 0.40 eV |
| Experimental $\Delta\mu$ (maximum temperature) | +15 meV (1100 K) | +15 meV (1026 K) |
| Expected $\Delta\mu$ (maximum temperature) | -38 meV (1100 K) | -33 meV (1026 K) |
| γ | $4.0 \pm 0.3 \text{ ps}^{-1}$ | $2.0 \pm 0.3 \text{ ps}^{-1}$ |
| G | $(9.3 \pm 0.1) \times 10^{13} \text{ cm}^{-2} \text{ ps}^{-1}$ | $(7.0 \pm 0.1) \times 10^{13} \text{ cm}^{-2} \text{ ps}^{-1}$ |

values between G and G_2 . Since the carrier doping in the single-layer graphene was observed on a vicinal substrate, the origin is seemingly related to the step region, shown in Fig. 7(a). Focusing on the atomic structure at the step edges, there are silicon and carbon atoms that are not terminated with the buffer layer. Thus it is inferred that the sources of the photoexcited carrier, doped to graphene layers, are electrons in such Si or C step-edge states at the interface.

To unveil the experimental facts that the transient doping is related to step states at the interface, Fig. 10(c) shows an energy diagram of the graphene/SiC interface based on the DFT calculation [36]. In the figure, photoexcitation by the optical pulse ($h\nu = 1.55 \text{ eV}$) is indicated by the arrows. The electronic structure around the Fermi level (μ_{eq}) is located within the SiC bulk band gap, and it is composed of the graphene Dirac bands and the interface Si dangling bonds (DBs). Since a band of the Si DB is unoccupied or located above μ_{eq} , the carrier source for the photoexcitation is only possible with the graphene Dirac bands in the ideal epitaxial system. This indicates the necessity of the extrinsic factor and that the atomic steps are inevitable defects at the interface. In the

actual interface, steps are distributed with a different interval or density depending on the crystal cut. On the actual flat SiC surface, the step interval is 1–2 μm , while it is 20 nm on the present vicinal surface (4° off-miscut), as shown in Figs. 10(a) and 10(b), respectively. While the accurate structure of the SiC steps has been controversial, there are systematic theoretical works that have calculated the possible electronic states at the step edges with Si and/or C atoms [37–41].

Figure 10(d) summarizes the DOS of various step edges at the SiC surface [37]. One can find that the step states are distributed in the SiC bulk band gap and have large DOS at the energy of 1–1.5 eV. This result apparently indicates a role of the carrier source of the optical doping. It is naturally inferred that electrons at the steps are transiently transferred to the epitaxial graphene and diffuse in the layer. Considering the carrier velocity of graphene, 10^6 m/s , the diffusion length can be estimated to be several tens of nanometers during the pumping time of the present pulse width. This length is long enough to instantly cover the epitaxial graphene with the transient electrons on the terrace of the vicinal SiC substrate [Fig. 10(b)]. This is consistent with the temporal behavior of $\Delta\mu$ in Fig. 9. On the other hand, it requires a longer time for diffusion on the wide terrace [Fig. 10(a)], and this dynamic restriction can be experimentally confirmed in Fig. 5. The results show a longer duration of the positive $\Delta\mu$ values in the LLD than the Dirac cone on the stepped substrate (Fig. 9). In addition, there is a delayed $\Delta\mu$ minimum in the ULD that can be explained by a balance between the negative shift caused by an intrinsic effect of the Dirac fermions and the positive shift caused by the external doping or diffusion of the step electrons. When the terrace is so large that the intralayer relaxation proceeds much earlier than the carrier diffusion over the terrace, one can observe the negative $\Delta\mu$ shift expected for the Dirac fermions. This naturally explains previous TARPES results of an epitaxial graphene layer on SiC [10].

These results comprehensively unveil roles of the substrate during the ultrafast carrier dynamics in epitaxial graphene. Electrons in the interface states, i.e., step edges, in the SiC bulk band gap can ballistically transfer to the graphene layer. The amount of transient carrier doping can be described by the spectral overlap of the wave-function tails that depends on the layer distance. In addition, the dynamics in subpicoseconds is governed by the subsequent carrier diffusion in the layer. The phenomenological parameter, G_i , in the rate equation is thus determined by the consequence of these stochastic processes. A combination of these elemental events likely induces the

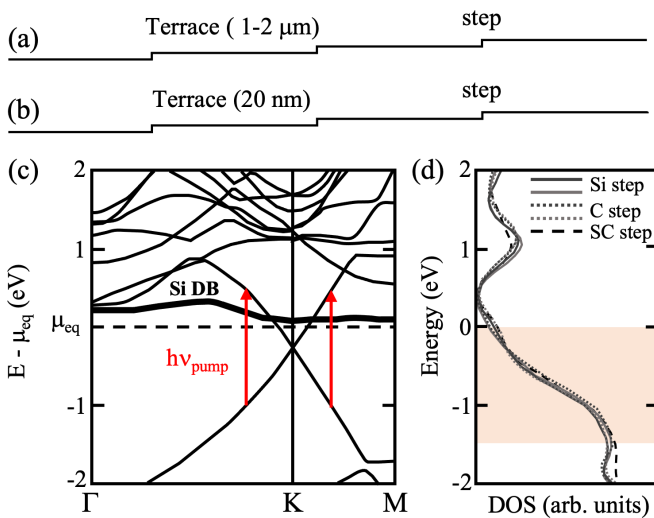


FIG. 10. (a) and (b) Schematic drawings of terraces and steps on the (a) flat and (b) stepped SiC surfaces. (c) Calculated band diagram of the epitaxial graphene layer on the SiC substrate [36]. (d) Density of states (DOS) of various atomic steps on the SiC surface [37–41]. A possible energy range of electronic states that can become sources of the optical doping is indicated by the shaded region.

dynamical phenomena of Dirac fermions, expected from free-standing graphene, or those specific to epitaxial graphene.

The present TARPES experiment revealed the existence of transient carrier doping from the interface. The results indicate that the epitaxial graphene layers are electronically sensitive to the environment, especially substrates or interfaces. This is mainly because the DOS of graphene in the meV region, $\sim 10^{11}$ – 10^{13} cm $^{-2}$, is much smaller than the atomic density at the interface, 10^{15} cm $^{-2}$. Therefore even defects at the interface can be critical in transient electronic changes in the overlayer. The SiC atomic step dealt with in this paper has an atomic density of $\sim 10^{12}$ – 10^{14} cm $^{-2}$, depending on the terrace size, which can be large enough to be a source of the carrier doping to the epitaxial graphene. This discussion provides an important aspect to understand the TARPES data, and it is also one of the possible explanations toward a complete understanding of the whole picture of carrier dynamics in graphene.

IV. CONCLUSION

TARPES measurements were conducted on various types of epitaxial graphene on SiC substrates to investigate the carrier dynamics. In QCBG, layer-dependent electron doping

was observed in the Dirac bands, generating transient voltage between the upper and lower layers. The phenomena were also found in single-layer graphene on a stepped SiC substrate and in nontwisted bilayer graphene. Based on the dynamical rate equation, the doping carriers likely originated from interface SiC states of the step edges. A comparison with the theoretical calculation unveils the dynamics role of the substrate that is responsible for the interface carrier transport and the subsequent diffusion in the overlayer. The present work opens a way to regulate carrier dynamics in graphene using these environmental effects to develop the next-generation optoelectronics.

ACKNOWLEDGMENTS

This work was supported by Grants-in-Aid for Specially Promoted Research (KAKENHI Grants No. JP18H03874, No. JP19H01818, No. JP19H04398, and No. JP21H05012) from Japan Society for the Promotion of Science and Grant No. NRF-2021M2E8A1048961 from the National Research Foundation (NRF) of Korea. We acknowledge Kaori Seino and Emi Minamitani for discussions on the theoretical calculations. The preliminary experiment was performed at facilities of the Synchrotron Radiation Research Organization, The University of Tokyo.

-
- [1] A. H. Castro Neto, F. Guinea, N. M. R. Peres, K. S. Novoselov, and A. K. Geim, *Rev. Mod. Phys.* **81**, 109 (2009).
- [2] F. Bonaccorso, Z. Sun, T. Hasan, and A. C. Ferrari, *Nat. Photonics* **4**, 611 (2010).
- [3] J. Wang, X. Mu, M. Sun, and T. Mu, *Appl. Mater. Today* **16**, 1 (2019).
- [4] Q. Bao, H. Hoh, and Y. Zhang, *Graphene Photonics, Optoelectronics, and Plasmonics* (Pan Stanford, Singapore, 2017).
- [5] M. Romagnoli, V. Soriano, M. Midrio *et al.*, *Nat. Rev. Mater.* **3**, 392 (2018).
- [6] S. A. Boubanga-Tombe, A. Satou, D. Yadav, D. B. But, W. Knap, V. V. Popov, I. V. Gorbenko, V. Kachorovskii, and T. Otsuji, *Front. Phys.* **9**, 726806 (2021).
- [7] V. Ryzhii, M. Ryzhii, V. Mitin, M. S. Shur, and T. Otsuji, *Phys. Rev. Appl.* **16**, 014001 (2021).
- [8] J. C. Johannsen, S. Ulstrup, F. Cilento, A. Crepaldi, M. Zacchigna, C. Cacho, I. C. Edmond Turcu, E. Springate, F. Fromm, C. Raidel, T. Seyller, F. Parmigiani, M. Grioni, and P. Hofmann, *Phys. Rev. Lett.* **111**, 027403 (2013).
- [9] T. Someya, H. Fukidome, H. Watanabe, T. Yamamoto, M. Okada, H. Suzuki, Y. Ogawa, T. Iimori, N. Ishii, T. Kanai, K. Tashima, B. Feng, S. Yamamoto, J. Itatani, F. Komori, K. Okazaki, S. Shin, and I. Matsuda, *Phys. Rev. B* **95**, 165303 (2017).
- [10] T. Someya, H. Fukidome, Y. Ishida, R. Yoshida, T. Iimori, R. Yukawa, K. Akikubo, Sh. Yamamoto, S. Yamamoto, T. Yamamoto, T. Kanai, K. Funakubo, M. Suemitsu, J. Itatani, F. Komori, S. Shin, and I. Matsuda, *Appl. Phys. Lett.* **104**, 161103 (2014).
- [11] I. Gierz, J. C. Petersen, M. Mitrano, C. Cacho, I. C. E. Turcu, E. Springate, A. Stöhr, A. Köhler, U. Starke, and A. Cavalleri, *Nat. Mater.* **12**, 1119 (2013).
- [12] S. Ulstrup, J. C. Johannsen, F. Cilento, J. A. Miwa, A. Crepaldi, M. Zacchigna, C. Cacho, R. Chapman, E. Springate, S. Mammadov, F. Fromm, C. Raidel, T. Seyller, F. Parmigiani, M. Grioni, P. D. C. King, and P. Hofmann, *Phys. Rev. Lett.* **112**, 257401 (2014).
- [13] T. Someya, H. Fukidome, N. Endo, K. Takahashi, S. Yamamoto, and I. Matsuda, *Appl. Phys. Lett.* **113**, 051601 (2018).
- [14] S. Yamamoto and I. Matsuda, *J. Phys. Soc. Jpn.* **82**, 021003 (2013).
- [15] Y. Cao, V. Fatemi, S. Fang, K. Watanabe, T. Taniguchi, E. Kaxiras, and P. Jarillo-Herrero, *Nature (London)* **556**, 43 (2018).
- [16] Y. Cao, V. Fatemi, A. Demir, S. Fang, S. L. Tomarken, J. Y. Luo, J. D. Sanchez-Yamagishi, K. Watanabe, T. Taniguchi, E. Kaxiras, R. C. Ashoori, and P. Jarillo-Herrero, *Nature (London)* **556**, 80 (2018).
- [17] S. J. Ahn, P. Moon, T. H. Kim, H. W. Kim, H. C. Shin, E. H. Kim, H. W. Cha, S. J. Kahng, P. Kim, M. Koshino, Y. W. Son, C. W. Yang, and J. R. Ahn, *Science* **361**, 782 (2018).
- [18] Y. Fukaya, Y. Zhao, H.-W. Kim, J. R. Ahn, H. Fukidome, and I. Matsuda, *Phys. Rev. B* **104**, L180202 (2021).
- [19] W. Yao, E. Wang, C. Bao, Y. Zhang, K. Zhang, K. Bao, C. K. Chan, C. Chen, J. Avila, M. C. Asensio, J. Zhu, and S. Zhou, *Proc. Natl. Acad. Sci. USA* **115**, 6928 (2018).
- [20] Y.-N. Ren, Y. Zhang, Y.-W. Liu, and L. He, *Chin. Phys. B* **29**, 117303 (2020).
- [21] T. Suzuki, T. Iimori, S. J. Ahn, Y. Zhao, M. Watanabe, J. Xu, M. Fujisawa, T. Kanai, N. Ishii, J. Itatani, K. Suwa, H. Fukidome, S. Tanaka, J. R. Ahn, K. Okazaki, S. Shin, F. Komori, and I. Matsuda, *ACS Nano* **13**, 11981 (2019).
- [22] J. D. Emery, V. D. Wheeler, J. E. Johns, M. E. McBriarty, B. Detlefs, M. C. Hersam, D. K. Gaskill, and M. J. Bedzyk, *Appl. Phys. Lett.* **105**, 161602 (2014).

- [23] T. Sumi, K. Nagai, J. Bao, T. Terasawa, W. Norimatsu, M. Kusunoki, and Y. Wakabayashi, *Appl. Phys. Lett.* **117**, 143102 (2020).
- [24] Y. Fukaya, I. Mochizuki, M. Maekawa, K. Wada, T. Hyodo, I. Matsuda, and A. Kawasuso, *Phys. Rev. B* **88**, 205413 (2013).
- [25] Y. Fukaya, I. Matsuda, B. Feng, I. Mochizuki, T. Hyodo, and S. Shamoto, *2D Mater.* **3**, 035019 (2016).
- [26] F. Owman and P. Martensson, *Surf. Sci.* **369**, 126 (1996).
- [27] L. Li and I. S. T. Tson, *Surf. Sci.* **351**, 141 (1996).
- [28] I. Forbeaux, J.-M. Themlin, A. Charrier, F. Thibaudau, and J.-M. Debever, *Appl. Surf. Sci.* **162-163**, 406 (2000).
- [29] A. Charrier, A. Coati, T. Argunova, F. Thibaudau, Y. Garreau, R. Pinchaux, I. Forbeaux, J.-M. Debever, M. Sauvage-Simkin, and J.-M. Themlin, *J. Appl. Phys. (Melville, NY)* **92**, 2479 (2002).
- [30] H. Fukidome, Y. Kawai, F. Fromm, M. Kotsugi, H. Handa, T. Ide, T. Ohkouchi, H. Miyashita, Y. Enta, T. Kinoshita, Th. Seyller, and M. Suemitsu, *Appl. Phys. Lett.* **101**, 041605 (2012).
- [31] N. Endoh, S. Akiyama, K. Tashima, K. Suwa, T. Kamogawa, R. Kohama, K. Funakubo, S. Konishi, H. Mogi, M. Kawahara, M. Kawai, Y. Kubota, T. Ohkochi, M. Kotsugi, K. Horiba, H. Kumigashira, M. Suemitsu, I. Watanabe, and H. Fukidome, *Nanomaterials* **11**, 392 (2021).
- [32] K. Kim, G. Park, H. Fukidome, S. Takashi, T. Iimori, F. Komori, I. Matsuda, and M. Suemitsu, *Carbon* **130**, 792 (2018).
- [33] K. Nakatsuji, Y. Shibata, R. Niikura, F. Komori, K. Morita, and S. Tanaka, *Phys. Rev. B* **82**, 045428 (2010).
- [34] T. Suzuki, S. Shin, and K. Okazaki, *J. Electron Spectrosc. Relat. Phenom.* **251**, 147105 (2021).
- [35] F. A. Chaves, D. Jiménez, A. W. Cummings, and S. Roche, *J. Appl. Phys. (Melville, NY)* **115**, 164513 (2014).
- [36] M. Kajihara, T. Suzuki, S. M. F. Shahed, T. Komeda, E. Minamitani, and S. Watanabe, *Surf. Sci.* **647**, 39 (2016).
- [37] K. Seino and A. Oshiyama, *Mater. Sci. Forum* **1004**, 145 (2020).
- [38] K. Seino and A. Oshiyama, *Phys. Rev. B* **101**, 195307 (2020).
- [39] K. Sawada, J. I. Iwata, and A. Oshiyama, *Phys. Rev. B* **93**, 235421 (2016).
- [40] K. Sawada, J. Iwata, and A. Oshiyama, *e-J. Surf. Sci. Nanotechnol.* **13**, 231 (2015).
- [41] K. Sawada, J. Iwata, and A. Oshiyama, *Appl. Phys. Lett.* **104**, 051605 (2014).